Quaternary Research (2017), **88**, 458–471.

doi:10.1017/qua.2017.72

Climatic and in-cave influences on $\delta^{18}O$ and $\delta^{13}C$ in a stalagmite from northeastern India through the last deglaciation

Franziska A. Lechleitner[a]*, Sebastian F.M. Breitenbach[a,b], Hai Cheng[c,d], Birgit Plessen[e], Kira Rehfeld[f], Bedartha Goswami[g,h], Norbert Marwan[g], Deniz Eroglu[g,i], Jess Adkins[j], Gerald Haug[a,k]

[a]Department of Earth Sciences, ETH Zurich, Sonneggstrasse 5, 8092 Zürich, Switzerland
[b]Sediment and Isotope Geology, Institute for Geology, Mineralogy & Geophysics, Ruhr-Universität Bochum, Universitätsstr. 150, 44801 Bochum, Germany
[c]Institute of Global Environmental Change, Xi'an Jiaotong University, Xi'an, 710054 Shaanxi, China
[d]Department of Earth Sciences, University of Minnesota, Minneapolis, Minnesota 55455, USA
[e]GFZ German Research Centre for Geosciences, 14473 Potsdam, Germany
[f]British Antarctic Survey, High Cross, Madingley Road, Cambridge CB3 0ET, United Kingdom
[g]Potsdam Institute for Climate Impact Research (PIK), 14412 Potsdam, Germany
[h]Institute for Earth and Environmental Science, University of Potsdam, Karl-Liebknecht-Str. 24-25, 14476 Potsdam, Germany
[i]Department of Physics, Humboldt-Universität zu Berlin, Newtonstr. 15, 12489 Berlin, Germany
[j]California Institute of Technology, Pasadena, California 91125, USA
[k]Department of Climate Geochemistry, Max Planck Institute for Chemistry, 55128 Mainz, Germany

(Received April 3, 2017; Accepted August 2, 2017)

Abstract

Northeastern (NE) India experiences extraordinarily pronounced seasonal climate, governed by the Indian summer monsoon (ISM). The vulnerability of this region to floods and droughts calls for detailed and highly resolved paleoclimate reconstructions to assess the recurrence rate and driving factors of ISM changes. We use stable oxygen and carbon isotope ratios ($\delta^{18}O$ and $\delta^{13}C$) from stalagmite MAW-6 from Mawmluh Cave to infer climate and environmental conditions in NE India over the last deglaciation (16–6 ka). We interpret stalagmite $\delta^{18}O$ as reflecting ISM strength, whereas $\delta^{13}C$ appears to be driven by local hydroclimate conditions. Pronounced shifts in ISM strength over the deglaciation are apparent from the $\delta^{18}O$ record, similarly to other records from monsoonal Asia. The ISM is weaker during the late glacial (LG) period and the Younger Dryas, and stronger during the Bølling-Allerød and Holocene. Local conditions inferred from the $\delta^{13}C$ record appear to have changed less substantially over time, possibly related to the masking effect of changing precipitation seasonality. Time series analysis of the $\delta^{18}O$ record reveals more chaotic conditions during the late glacial and higher predictability during the Holocene, likely related to the strengthening of the seasonal recurrence of the ISM with the onset of the Holocene.

Keywords: Indian Summer Monsoon; stalagmite; oxygen isotopes; carbon isotopes; deglaciation

INTRODUCTION

The Asian monsoon (AM) is characterized by the seasonal reversal of circulation between ocean and landmasses throughout Southeast Asia, resulting in pronounced hydroclimate seasonality in the affected regions. Stalagmite oxygen isotope ratio ($\delta^{18}O$) records from the AM realm have provided crucial information on past climate conditions in this densely populated region (e.g., Wang et al., 2005; Cheng et al., 2016a; Eroglu et al., 2016). Pronounced glacial-interglacial variations in AM strength are found to be strongly influenced by Northern Hemisphere summer insolation (Cheng et al., 2009, 2016a; Kathayat et al., 2016) and closely related to changes in the North Atlantic (Wang et al., 2001; Yuan et al., 2004). The AM is therefore a highly dynamic system susceptible to external and internal forcings, calling for precise paleoclimate reconstructions throughout monsoonal Asia to infer future developments under climate change scenarios.

The majority of precisely dated high-resolution reconstructions of past glacial-interglacial AM variation stem from Chinese caves, providing unprecedented insight into monsoonal dynamics over the past 640,000 yr (Cheng et al., 2016a). Information from the Indian subcontinent, particularly at high temporal resolution and chronological precision, is still relatively scarce over these time scales (e.g., Sinha et al., 2005; Govil and Divakar Naidu, 2011; Zhisheng et al., 2011; Menzel et al., 2014; Kathayat et al., 2016). The Indian

*Corresponding author at: Department of Earth Sciences, University of Oxford, South Parks Road, Oxford OX1 3AN, United Kingdom. E-mail address: franziska.lechleitner@earth.ox.ac.uk (F.A. Lechleitner).

summer monsoon (ISM) is the branch of the AM that delivers moisture from the Arabian Sea and Indian Ocean to the Indian subcontinent, as well as to the Arabian peninsula (Burns et al., 2002; Fleitmann et al., 2007), and China (Zhisheng et al., 2011; Baker et al., 2015). It delivers ~80% of the annual rainfall of these regions and dominates their hydrologic cycle (Sinha et al., 2007, Breitenbach et al. 2010) (Fig. 1A).

Stalagmite $\delta^{18}O$ is a widely applied proxy for monsoonal strength in Asia and is interpreted as reflecting the $\delta^{18}O$ of precipitation (Breitenbach et al., 2010, 2015; Pausata et al., 2011; Cheng et al., 2016b; Eroglu et al., 2016). As the $\delta^{18}O$ signal is governed by a multitude of factors, their relative importance at a specific location needs to be carefully assessed to correctly interpret paleoclimatic data. Isotopic composition of the moisture source, transport length, and the amount of precipitation at the site can all affect precipitation $\delta^{18}O$ in monsoonal regions, and taken together, they provide information on monsoonal strength (Breitenbach et al., 2010; Baker et al., 2015; Eroglu et al., 2016). Cave monitoring efforts and simultaneous study of different stalagmite geochemical proxies in parallel often allow researchers to more clearly determine the controls on local climate conditions, leading to more accurate paleoclimate reconstructions (Baldini, 2010; Oster et al., 2012; Breitenbach et al., 2015; Baldini et al., 2016; Cheng et al., 2016b). Stable carbon isotope ratios ($\delta^{13}C$) are routinely measured together with $\delta^{18}O$ but have so far rarely been reported for records from monsoonal Asia. This is partly because of the more complicated and site-specific interpretation of stalagmite $\delta^{13}C$, which necessitates thorough understanding of the local conditions; $\delta^{13}C$ can be influenced by vegetation composition (i.e., C_3 vs. C_4 plants), soil processes, open versus closed conditions in the karst during carbonate dissolution, and isotope fractionation in or above the cave (Fairchild and Baker, 2012). However, carefully evaluated stalagmite $\delta^{13}C$ time series can provide important climate information to supplement and extend the interpretation of $\delta^{18}O$ records, often resulting in a more in-depth understanding of past climate conditions (Genty et al., 2003; Cosford et al., 2009; Ridley et al., 2015; Cheng et al., 2016b). Particularly interesting is the difference in spatial scale between both proxies: $\delta^{18}O$ generally reflects large-scale atmospheric circulation processes (Breitenbach et al., 2010; Baker et al., 2015), whereas $\delta^{13}C$ is a proxy for local processes and is therefore more sensitive to changes at local to regional levels (Ridley et al., 2015; Cheng et al., 2016b).

Here, we present new subdecadally resolved $\delta^{18}O$ and $\delta^{13}C$ data from a stalagmite from NE India that cover the interval of the last deglaciation and early Holocene (EH; ~16–6.5 ka). The last deglaciation was a period of rapid and substantial global climate change, driven by a ~3.5°C increase in global temperatures (Shakun et al., 2012). This resulted in large-scale reorganizations of circulation and weather patterns globally, with important repercussions in monsoonal Asia (Dykoski et al., 2005; Cheng et al., 2009; Ma et al., 2012). This analysis follows long-term studies of the controls on precipitation $\delta^{18}O$ (Breitenbach et al., 2010), as well as detailed cave microclimate monitoring schemes (Breitenbach et al., 2015), which allow us to disentangle local and regional responses to climate change over the last deglaciation.

GEOGRAPHIC AND CLIMATOLOGICAL SETTING

Mawmluh Cave is located at 25.26°N, 91.88°E, 1320 m above sea level on the Meghalaya Plateau in NE India (Fig. 1). The cave developed in a Tertiary limestone butte at the southern fringe of the plateau (Ghosh et al., 2005; Gebauer, 2008) and is today mainly covered by grassland. Mean annual air temperature inside the cave (18.5°C) is very similar to that recorded at the meteorological station Cherrapunji (17.4°C) and in the nearby Mawmluh village (19.1°C).

Hydroclimate in Meghalaya is extremely seasonal, with ~80% of annual precipitation falling during the ISM season (June–October; Breitenbach et al., 2010). The Meghalaya Plateau is the first morphological barrier for northward-moving moisture from the Bay of Bengal (BoB), inducing intense orographic rainfall. Thus, Meghalaya is a major water source for the Bangladesh plains, a region frequently flooded during summer—for example, in 1998, when ~60% of the country was inundated (Murata et al., 2008; Webster, 2013). Despite having the highest rainfall amount in the world (Prokop and Walanus, 2003), low retention capacity, because of the geologic conditions on the southern Meghalaya Plateau, results in frequent water shortage during the dry season (November–May).

MATERIALS AND METHODS

Stalagmite MAW-6

The 21-cm-long stalagmite MAW-6 was found broken in Mawmluh Cave in 2009, and its original position is known only approximately (Fig. 1). The stalagmite displays complex brown-gray color variations, with bands up to a few millimeters wide, but no annual laminations. At least three white layers can be discerned, which span from the growth axis toward the sides of the stalagmite. To verify the mineralogy in MAW-6, three samples were analyzed by X-ray diffraction (XRD) using a powder XRD diffractometer (Bruker, D8 Advance), equipped with a scintillation counter and an automatic sampler at ETH Zurich, Switzerland.

U-series dating and chronology development

After cutting the stalagmite lengthwise using a diamond stone saw, 24 U-series samples with weights between 88 and 311 mg were milled using an ethanol-cleaned stainless steel bit and subsequently analyzed by multicollector inductively coupled plasma mass spectrometry using a Thermo-Finnigan Neptune in the Minnesota isotope laboratory, University of Minnesota. The chemical procedures used to separate uranium and thorium for U-series dating are similar to those

https://doi.org/10.1017/qua.2017.72 Published online by Cambridge University Press

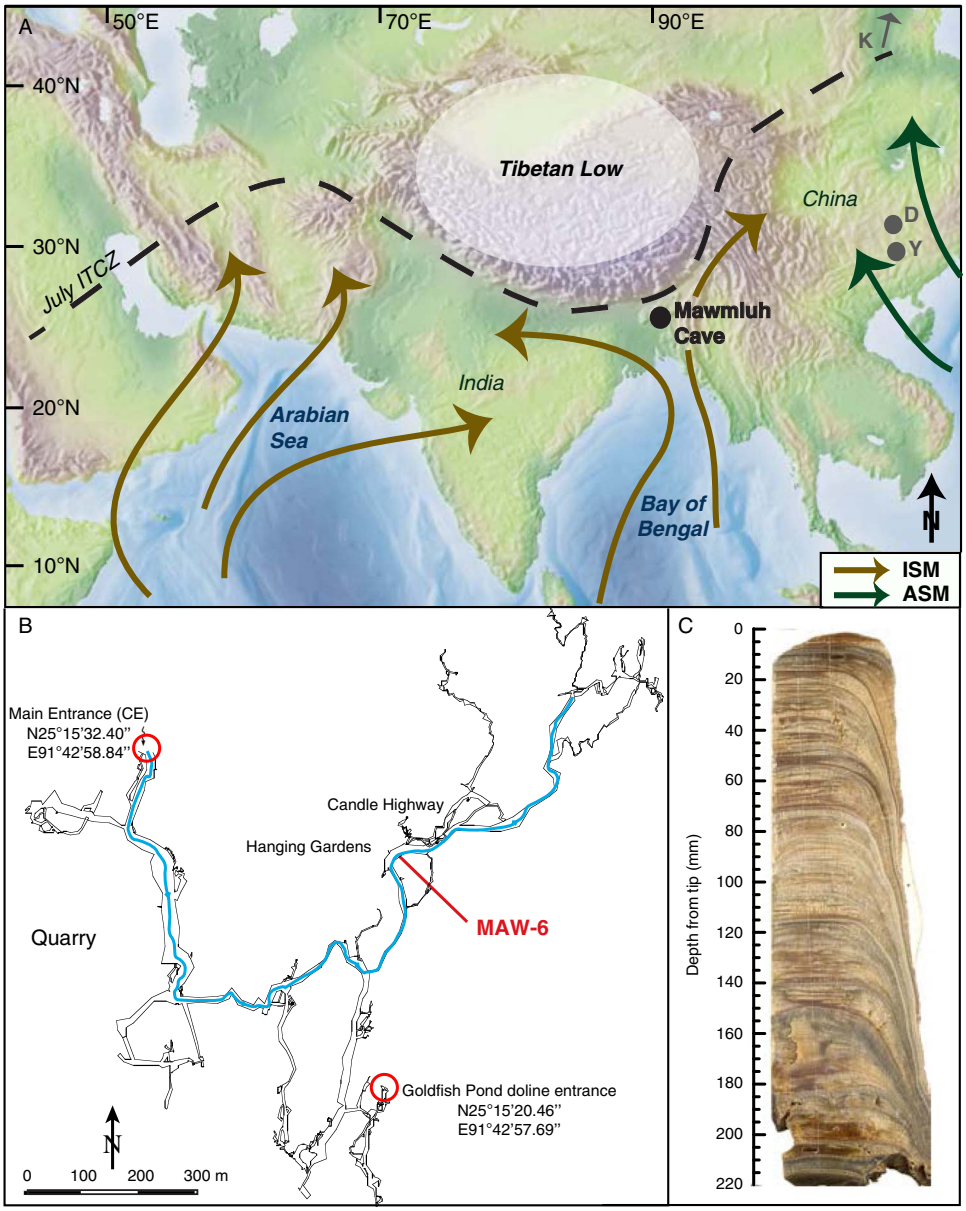

Figure 1. (A) Map with summer climatological conditions in the broader study area. The location of Mawmluh Cave in northeastern India is indicated by the black dot. Other discussed cave locations are indicated by the gray dots and arrows (D, Dongge Cave; K, Kulishu Cave; Y, Yamen Cave). The dashed line indicates maximum northward extent of the Intertropical Convergence Zone (ITCZ), which drives monsoonal circulation. Brown arrows delineate dominant Indian summer monsoon (ISM) circulation patterns; Asian summer monsoon (ASM) winds are shown in green. (B) Map of Mawmluh Cave. Stalagmite MAW-6 was found broken in the West Stream (map courtesy of Daniel Gebauer). (C) Scan of cut and polished stalagmite MAW-6. (For interpretation of the references to color in this figure legend, the reader is referred to the web version of this article.)

described in Edwards et al. (1987). Uranium and thorium isotopes were analyzed on the multiplier behind the retarding potential quadrupole in peak-jumping mode. Instrumental mass fractionation was determined by measurements of a $^{233}U/^{236}U$ spike. The detail techniques are similar to those described by Cheng et al. (2000, 2009), and half-life values are those reported by Cheng et al. (2013).

The age model for MAW-6 was computed for each growth segment by applying a cubic interpolation procedure using the COPRA software (Breitenbach et al., 2012). COPRA computed 2000 ensemble realizations for both the $\delta^{18}O$ and $\delta^{13}C$ records, from which the median (i.e., the central age for a defined sample depth) was calculated. The uncertainty in the age model is defined by the 95% confidence intervals, derived using the $\pm 2\sigma$ deviation from the median (Breitenbach et al., 2012).

Stable isotope analysis

One thousand and fifty samples for stable isotope analysis were milled continuously at 200 µm resolution using a semiautomated high-precision drill (Sherline 5400 Deluxe) at ETH Zurich. Nine

https://doi.org/10.1017/qua.2017.72 Published online by Cambridge University Press

Hendy tests were performed over the length of the stalagmite to look for signs of kinetic isotope fractionation effects and, if present, to evaluate potential changes in the intensity of kinetic fractionation through time (Supplementary Fig. 1). For this, carbonate samples were drilled point-wise along a single layer of the stalagmite using a 0.3-mm-diameter drill bit.

Samples were analyzed for $\delta^{18}O$ and $\delta^{13}C$ on a Delta V Plus mass spectrometer coupled to a ThermoFinnigan GasBench II carbonate preparation device at the Geological Institute, ETH Zurich (Breitenbach and Bernasconi, 2011). An in-house carbonate standard (MS2), which is well linked to NBS19 (Breitenbach and Bernasconi, 2011), was used to evaluate the runs. All values are expressed in per mil (‰) and referenced to the Vienna Pee Dee belemnite standard. The external standard deviation (1σ) for both $\delta^{18}O$ and $\delta^{13}C$ analyses on the carbonate is smaller than 0.07‰.

Because the MAW-6 record covers the period of the last deglaciation, the contribution of changes in both sea surface temperature (SST) and sea level because of the melting of continental ice sheets to stalagmite $\delta^{18}O$ must be considered. To estimate this contribution, a linear interpolation of seawater $\delta^{18}O$ values ($\delta^{18}O_{seawater}$) reconstructed from a sediment core from the BoB (Rashid et al., 2011) was performed to fit the MAW-6 data points. The $\delta^{18}O_{seawater}$ record was subsequently subtracted from the measured $\delta^{18}O_{calcite}$ in MAW-6, to yield an ice-volume-corrected ($\delta^{18}O_{IVC}$) record (Supplementary Fig. 2). It should be noted that this procedure can introduce artifacts, as the records are irregularly sampled, and the results should be interpreted with care.

Recurrence quantification analysis

To infer possible changes in the dynamic regime of the ISM between late glacial (LG) and EH conditions, we performed a statistical analysis considering the deterministic nature of the underlying process (the ISM), encoded by the recurrence properties of the $\delta^{18}O_{IVC}$ record. We use a measure of complexity, called *recurrence determinism* (DET), which is derived from a recurrence plot, a graphic, binary representation of pairs of times of similar values (actually states) within the time series (see Supplementary Materials for further details; Marwan et al., 2007; Ozken et al., 2015; Eroglu et al., 2016). DET reveals high values for deterministic processes and regular (e.g., cyclic, periodic) variations, whereas more stochastic (i.e., random) dynamics lead to low DET values. Moreover, the recurrence analysis is combined with the preprocessing Transformation-Cost Time-Series (TACTS) technique that allows detrending regularization of irregularly sampled time series (see Supplementary Materials; Ozken et al., 2015).

The $\delta^{18}O_{IVC}$ record was divided into two periods, the LG period (16–13 ka) and the EH (9–6.5 ka), and the DET measures were calculated for both periods separately. A statistical test based on a bootstrap approach was performed to evaluate the significance of the variations in the DET measure. This test provides a cumulative probability distribution of DET measures corresponding to the null hypothesis that there is no change in the dynamics of the underlying climate process. From this test distribution, the upper 95% confidence limit can be defined.

RESULTS

Petrography and mineralogy

XRD analysis reveals that stalagmite MAW-6 consists of calcite. The white layers described previously were identified as dirt layers in the stalagmite. They are well visible at the fringes of the respective layers, and the stalagmite tip has been washed clean by impinging water droplets (Fig. 1C). The deposition of silty material on the stalagmite surface at these depths might indicate burial of MAW-6 by sediment redeposition in the cave, inhibiting further growth. Several buried stalagmites have been located in the cave (Supplementary Fig. 3), and sediment migration within the cave passage appears to be an important process during high-discharge events of the cave stream. However, caution must be applied with this interpretation because dirt layers can also originate from other processes, such as aerosol and dust deposition.

Age model

MAW-6 grew between ~16 and 6.5 ka. The age model is based on 20 U-series dates, with analytical errors between ±16 and ±264 yr (Fig. 2, Table 1). Four dating samples contained high amounts of detrital thorium and were excluded from the final age model (shown in red in Fig. 2).

Three hiatuses were identified in the depth-age relationship, coinciding with the white dirt layers in the stalagmite. User-specified hiatus depths of 69.46, 111.86, and 147.26 mm from the stalagmite top allowed COPRA to split the age model construction into independent age models (before and after the hiatuses, respectively). This procedure yielded a segmented depth-age chronology for the stalagmite, with hiatuses at 10.4–9.6, 11.6–10.8, and 13–12.4 ka. The details for the age-modeling procedure can be found in Breitenbach et al. (2012).

Using the COPRA procedure, the age uncertainties of the MAW-6 record can be transferred from the age to the proxy domain (Breitenbach et al., 2012), which results in a 95% confidence interval of possible proxy values at a given point in time. As a consequence, it is not possible to determine the high-frequency variations within the bounds of the confidence interval (Fig. 3A). Comparative discussions with other paleoclimate records from the AM realm are therefore restricted to the median proxy values in MAW-6 derived from the COPRA Monte Carlo modeling and to long-term centennial changes. We still show the original MAW-6 isotope data for a tentative comparison with other available records in (see discussion), as this kind of uncertainty is common to all paleoclimate records.

The MAW-6 $\delta^{18}O$ and $\delta^{13}C$ records

The $\delta^{18}O$ profile varies from −8.3‰ to −2.8‰ (Fig. 3A), with heavier values found in the oldest part of the record (end

https://doi.org/10.1017/qua.2017.72 Published online by Cambridge University Press

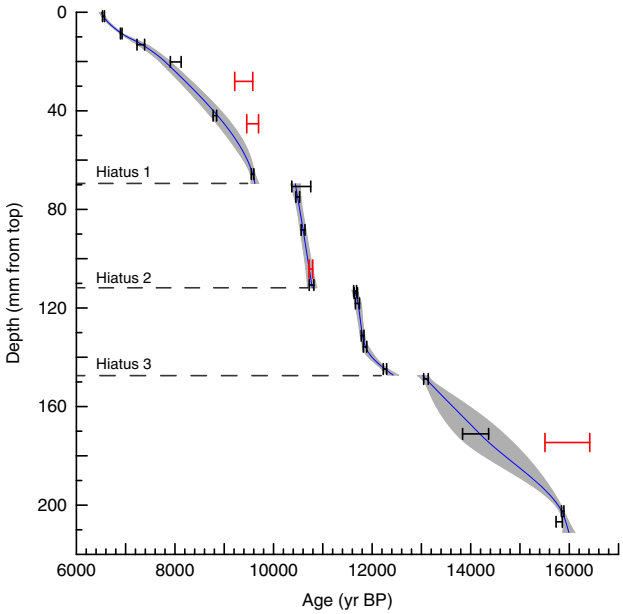

Figure 2. Age model of MAW-6 (constructed using cubic interpolation in COPRA). The median of the age model is shown in blue, with the 95% confidence intervals in light gray. The U-series ages used to construct the age model are shown in black, and the excluded ages are in red. Hiatuses are indicated by dashed black lines. (For interpretation of the references to color in this figure legend, the reader is referred to the web version of this article.)

of the last glacial period), and lighter values in the youngest part (the Holocene). Both, the Bølling-Allerød (B-A) interstadial period, beginning at ~14.5 ka with −1.5‰ shift, and the Younger Dryas (YD), between 12.6 and 11.6 ka and featuring the heaviest values of the entire record (approximately −3.5‰), are clearly demarcated. However, the exact beginning and the end of the YD in MAW-6 cannot be defined because the interval is bracketed by two hiatuses. The 850-yr-long hiatus that masks the end of the YD is followed by a substantial 4.5‰ decrease in $\delta^{18}O$, marking the transition into the Holocene (~9.6 ka). This decrease occurs in two rapid stages, characterized by hiatuses, interrupted by an interval (~10.8–10.2 ka) of relatively constant intermediate values (approximately −6.5‰). Lowest $\delta^{18}O$ values (~ −8‰) are found during the EH (~9.6 ka), slightly increasing toward the youngest part of the record. Our sea-level-corrected $\delta^{18}O_{IVC}$ record shows that ice volume and SST changes affect the isotope signature mainly before the YD, with only minor impacts during the Holocene, accounting for ~1/4 (1‰) of the shift between deglaciation and Holocene (Fig. 3A). We are therefore confident that the larger part (3‰) of the variation in $\delta^{18}O$ during the deglaciation is attributable to changes in ISM strength. For the following discussion, only the $\delta^{18}O_{IVC}$ record is considered.

Compared with the $\delta^{18}O$ profile, the $\delta^{13}C$ profile is much more uniform, with variations ranging between −1.2‰ and −6.6‰ and without clear trends over time. The heaviest values are found during the early part of the record (LG/B-A, average −4‰). In contrast to $\delta^{18}O$, the YD period is characterized by slightly lighter values than during the LG/B-A section (average −4.3‰), whereas the transition into the Holocene leads to the most negative values (average −5.2‰ post ~9.6 ka). The high-frequency variations in $\delta^{18}O$ and $\delta^{13}C$ are remarkably similar, but shifts in $\delta^{13}C$ are generally much more pronounced than in $\delta^{18}O$. The similarity between the two records is also reflected by their high correlation (during all periods, $r > 0.55$; Fig. 3B).

A cross plot of $\delta^{13}C$ versus $\delta^{18}O_{IVC}$ reveals four distinct clusters (Fig. 4). These clusters are mainly influenced by the average $\delta^{18}O_{IVC}$ during the different periods; therefore, we distinguish Holocene, intermediate (10.8–10.2 ka), YD, and B-A/LG clusters. The box plot representation of the data sets in Figure 4B allows the quantification of temporal and proxy-related differences. Although a clear distinction of the different time periods is apparent in the $\delta^{18}O_{IVC}$ data set, a much larger spread in $\delta^{13}C$ values is found (Fig. 4B). The YD cluster is characterized by the heaviest $\delta^{18}O_{IVC}$ values of the entire record, whereas $\delta^{13}C$ is slightly lighter than during the LG period. A trend toward progressively lighter $\delta^{18}O_{IVC}$ values is found between the YD, intermediate, and Holocene clusters, whereas intermediate $\delta^{13}C$ values are slightly heavier than during the YD (Fig. 4B).

The Hendy tests carried out throughout MAW-6 show evidence for kinetic fractionation during the YD and the LG period, whereas (near-) equilibrium conditions seem to have prevailed during the B-A and the Holocene (Supplementary Fig. 1). Kinetic effects are identified by strong correlations between $\delta^{18}O$ and $\delta^{13}C$, as well as enrichment in the heavy isotopes with increasing distance from the growth axis (Hendy, 1971).

Determinism of the $\delta^{18}O$ record

The analysis reveals distinctly different DET measures for the LG (DET = 0.663, inside the confidence interval) and the EH (DET = 0.736, outside the confidence interval). A high DET measure indicates a more predictable (i.e., a less chaotic) regime, whereas the opposite holds true for low DET measures.

DISCUSSION

Influence of karst processes on stalagmite stable isotopes in Mawmluh Cave

Karst processes at Mawmluh Cave are driven by the seasonal cycle in regional hydrology (Fig. 5). Precipitation $\delta^{18}O$ becomes increasingly lighter during the ISM months and reaches the most negative values during the late and post-ISM (August–October) (Breitenbach et al., 2010). A direct amount effect can therefore be ruled out, as maximum precipitation occurs earlier in the ISM season (July–August). Instead, precipitation $\delta^{18}O$ in Meghalaya is controlled by the following: (1) the travel distance of the air masses, which

https://doi.org/10.1017/qua.2017.72 Published online by Cambridge University Press

Table 1. U-series dating results for stalagmite MAW-6. The errors given are 2σ. Corrected ^{230}Th ages assume the initial ^{230}Th/^{232}Th atomic ratio of $4.4 \pm 2.2 \times 10^{-6}$. Those are the values for a material at secular equilibrium, with the bulk earth ^{232}Th/^{238}U value of 3.8. The errors are arbitrarily assumed to be 50%. Values are indicated at one decimal place more than significant, to avoid rounding errors. Ages excluded from the final chronology are shown in italics.

Sample ID	Depth (mm from top)	^{238}U (ppb)	^{232}Th (ppt)	^{230}Th/^{232}Th (atomic × 10^{-6})	$\delta^{234}U^{a}$ (measured)	^{230}Th/^{238}U (activity)	^{230}Th age (yr) (uncorrected)	^{230}Th age (yr BP)[b] (corrected)	$\delta^{234}U_{initial}$[c] (corrected)
MAW-6_U24	1.6	1565 ± 2	427 ± 9	3074 ± 63	−135.4 ± 1.3	0.0509 ± 0.0001	6621 ± 18	6550 ± 19	−138 ± 1
MAW-6_U1	8.6	1483 1.3	121 ± 54	10,665 ± 4776	−143.9 ± 0.5	0.0529 ± 0.0001	6973 ± 15	6910 ± 16	−147 ± 1
MAW-6_U3	13.1	1402 ± 2	4196 ± 84	310 ± 6.3	−147.3 ± 1.8	0.0564 ± 0.0002	7470 ± 26	7307 ± 77	−150 ± 2
MAW-6_U23	20.2	1030 ± 1	4514 ± 90	236 ± 5	−136.3 ± 1.3	0.0626 ± 0.0002	8227 ± 32	8016 ± 110	−139 ± 1
MAW-6_U4	*28.05*	*1340 ± 2*	*10,081 ± 202*	*162.7 ± 3.3*	*−126.6 ± 2.2*	*0.0742 ± 0.0002*	*9708 ± 42*	*9396 ± 183*	*−130 ± 2*
MAW-6_U5	42.0	1448 ± 2	826 ± 17	1996 ± 40.4	−116.2 ± 2.1	0.0691 ± 0.0002	8889 ± 33	8810 ± 35	−119 ± 2
MAW-6_U6	*45.26*	*1087 ± 2*	*4916 ± 99*	*271.8 ± 5.6*	*−129.9 ± 2.4*	*0.0746 ± 0.0003*	*9788 ± 53*	*9576 ± 120*	*−133 ± 2*
MAW-6_U7	65.7	1025 ± 1	342 ± 7	3737 ± 76	−106.3 ± 1.2	0.0755 ± 0.0001	9646 ± 24	9575 ± 25	−109 ± 1
MAW-6_U8	70.7	812 ± 1	6648 ± 133	171 ± 3	−106.8 ± 1.4	0.0848 ± 0.0002	10,892 ± 31	10,563 ± 192	−110 ± 1
MAW-6_U22	74.9	851 ± 1	349 ± 7	3299 ± 71	−109.4 ± 1.4	0.0821 ± 0.0002	10,567 ± 36	10,492 ± 38	−113 ± 1
MAW-6_U9	88.3	836 ± 1	711 ± 14	1617 ± 33	−104.7 ± 1.4	0.0834 ± 0.0002	10,687 ± 33	10,599 ± 38	−108 ± 1
MAW-6_U21	*104.18*	*712 ± 1*	*3619 ± 73*	*277 ± 6*	*−105.6 ± 1.3*	*0.0856 ± 0.0004*	*10,985 ± 51*	*10,757 ± 38*	*−109 ± 1*
MAW-6_U10	110.7	901 ± 1	1145 ± 23	1100 ± 22	−105.5 ± 1.6	0.0847 ± 0.0002	10,873 ± 37	10,772 ± 47	−109 ± 2
MAW-6_U20	113.1	1514 ± 2	945 ± 19	2414 ± 49	−103.4 ± 1.2	0.0913 ± 0.0002	11,738 ± 26	11,655 ± 30	−107 ± 1
MAW-6_U11	114.0	1289 ± 2	801 ± 16	2416 ± 49	−106.8 ± 1.3	0.0911 ± 0.0002	11,751 ± 32	11,670 ± 35	−110 ± 1
MAW-6_U19	118.2	984 ± 1	633 ± 13	2343 ± 49	−106.9 ± 1.3	0.0913 ± 0.0002	11,786 ± 38	11,703 ± 41	−111 ± 1
MAW-6_U18	131.2	1653 ± 2	601 ± 12	4224 ± 85	−96.5 ± 1.2	0.0931 ± 0.0001	11,882 ± 26	11,808 ± 27	−100 ± 1
MAW-6_U12	135.7	1904 ± 3	720 ± 14	4050 ± 82	−101.6 ± 1.5	0.0929 ± 0.0002	11,930 ± 34	11,857 ± 35	−105 ± 2
MAW-6_U13	144.8	2146 ± 3	725 ± 15	4634 ± 93	−110.8 ± 1.4	0.0949 ± 0.0002	12,332 ± 33	12,261 ± 34	−115 ± 1
MAW-6_U14	148.8	1589 ± 2	2149 ± 43	1204 ± 24	−131.3 ± 1.3	0.0988 ± 0.0002	13,199 ± 33	13,093 ± 46	−136 ± 1
MAW-6_U17	171.1	1548 ± 3	17,361 ± 348	164 ± 3.3	−106.1 ± 1.7	0.1112 ± 0.0003	14,530 ± 48	14,100 ± 264	−110 ± 2
MAW-6_U15	*174.60*	*1319 ± 2*	*25,078 ± 502*	*107 ± 2*	*−123.0 ± 1.4*	*0.1238 ± 0.0004*	*16,659 ± 59*	*15,962 ± 454*	*−129 ± 1*
MAW-6_U2	202.5	1171 1.0	116 ± 27	19,869 ± 9120	−117.4 ± 0.6	0.1198 ± 0.0002	15,927 ± 24	15,867 ± 24	−123 ± 1
MAW-6_U16	206.8	1179 ± 2	2267 ± 45	1008 ± 20.3	−132.3 ± 1.5	0.1175 ± 0.0002	15,923 ± 44	15,796 ± 63	−138 ± 2

[a] $\delta^{234}U = ([^{234}U/^{238}U]_{activity} - 1) \times 1000$.
[b] BP stands for "before present" where the "present" is defined as the year AD 1950.
[c] $\delta^{234}U_{initial}$ was calculated based on ^{230}Th age (T) (i.e., $\delta^{234}U_{initial} = \delta^{234}U_{measured} \times e^{\lambda 234 \times T}$).

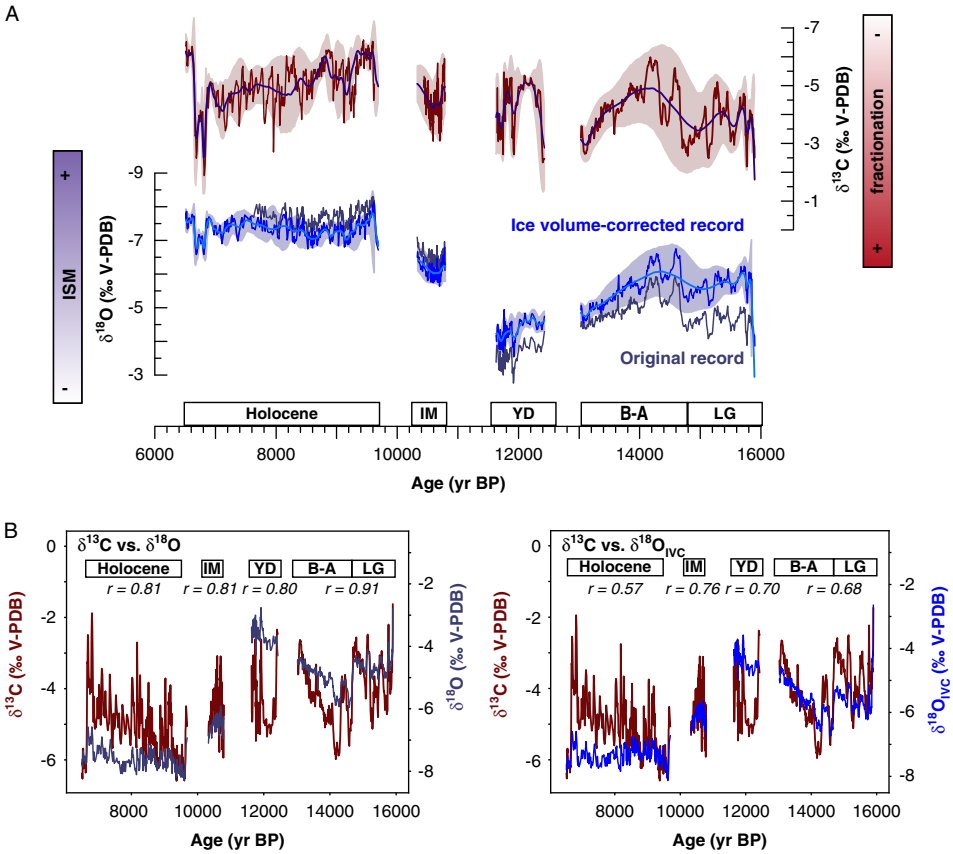

Figure 3. (color online) (A) $\delta^{18}O$ and $\delta^{13}C$ records with median and 95% confidence intervals. The time periods discussed in this study are indicated at the bottom of the figure (B-A, Bølling-Allerød; IM, intermediate period, 10.8–10.2 ka; LG, late glacial; YD, Younger Dryas). Major controls on $\delta^{18}O$ (Indian summer monsoon [ISM] strength) and $\delta^{13}C$ (amount of in-cave fractionation as a result of cave air pCO_2 and drip rate) are indicated by the bars. (B) Cross correlation between $\delta^{18}O$ and ice-volume-corrected $\delta^{18}O$ ($\delta^{18}O_{IVC}$) versus $\delta^{13}C$, estimated using kernel-based cross correlation analysis (Rehfeld and Kurths, 2014) with the toolbox NESTool (http://tocsy.pik-potsdam.de/nest.php). V-PDB, Vienna Pee Dee belemnite.

increases throughout the ISM season, promoting stronger Rayleigh fractionation during transport and lighter $\delta^{18}O$ at the site (Breitenbach et al., 2010); (2) stronger contribution from isotopically depleted freshwater delivered to the BoB during the late ISM (Sengupta and Sarkar, 2006; Singh et al., 2007; Breitenbach et al., 2010); and (3) isotopic depletion of rainwater during large rainstorms (amount effect sensu Dansgaard, 1964) (Lawrence et al., 2004; Breitenbach et al., 2010; Baker et al., 2015). These mechanisms all drive precipitation $\delta^{18}O$ in the same direction, resulting in lighter $\delta^{18}O$ during and after the ISM and heavier values during dry season months (Breitenbach et al., 2015; Myers et al., 2015). At Mawmluh Cave, infiltration is strongly skewed toward the summer months, and consequently, drip water $\delta^{18}O$ is biased toward the ISM season (Fig. 5). Still, a clear seasonal cycle in drip water $\delta^{18}O$ is observed, with the lightest values occurring during the late ISM months, indicating rapid (<1 month) fluid transfer into the cave (Breitenbach et al., 2015) (Fig. 5). Drip water (and stalagmite) $\delta^{18}O$ at Mawmluh Cave can therefore be used as a reliable ISM strength proxy.

Drip water $\delta^{13}C$ can be influenced by changes in vegetation type above the cave (C_3 vs. C_4 plants; Denniston et al., 2001), soil activity (Genty et al., 2006; Scholz et al., 2012), bedrock dissolution and open versus closed system conditions in the karst (Genty et al., 2001), and prior calcite precipitation Prior calcite precipitation is correct (PCP). and fractionation processes in the cave (Griffiths et al., 2012; Ridley et al., 2015). At Mawmluh Cave, precipitation and consequently vegetation and soil activity (microbial activity and root respiration) are at a maximum during the summer months (June–October), resulting in highest relative humidity and soil pCO_2 during this period. The extremely high amounts of rainfall delivered at Mawmluh Cave during the ISM season (max. 13,472 mm between June and September; Breitenbach et al., 2015) lead to waterlogging of the soil and karst overlying the cave (Breitenbach et al., 2015), most likely resulting in more closed system conditions. Therefore, PCP in epikarst and cave is minimized (or even completely absent) during the ISM season. Strong seasonal variations in cave air pCO_2 are observed as a consequence of seasonal ventilation changes (Breitenbach et al., 2015) (Fig. 5). During the dry season months, low cave air pCO_2 attributable to strongly reduced rainfall amount above the cave and intensified ventilation, leads to enhanced degassing of CO_2 from the solution, enriching drip water in ^{13}C (Breitenbach et al., 2015). Moreover, open system conditions

https://doi.org/10.1017/qua.2017.72 Published online by Cambridge University Press

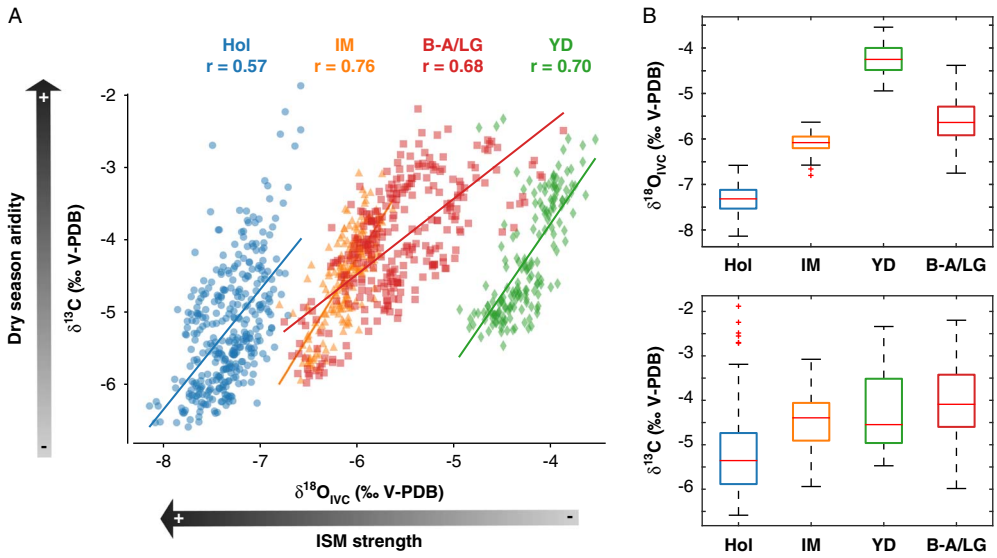

Figure 4. (A) $\delta^{13}C$ versus ice-volume-corrected $\delta^{18}O$ ($\delta^{18}O_{IVC}$) relationship in stalagmite MAW-6. The record can be subdivided into clusters corresponding to different time periods: Holocene (Hol), intermediate (IM), Younger Dryas (YD), and Bølling-Allerød and late glacial (B-A/LG). All clusters show high degrees of correlation between $\delta^{13}C$ and $\delta^{18}O_{IVC}$, indicated by the corresponding *r* values (same values as in Fig. 3B). Arrows indicate the direction of the main forcings (dry season aridity and Indian summer monsoon [ISM] strength). (B) Boxplots for $\delta^{18}O_{IVC}$ and $\delta^{13}C$ (top and bottom panels, respectively). Boxes are defined by the median (red line) and delimited by the first and third quartiles. Whiskers define the lowest and highest values within 1.5 times the interquartile range of the cluster. Outliers are indicated by red crosses. V-PDB, Vienna Pee Dee belemnite. (For interpretation of the references to color in this figure legend, the reader is referred to the web version of this article.)

prevail in the overlying soil and karst, because of seasonal aridity, resulting in low soil activity (less input of isotopically light organic carbon to soil water) and promoting PCP (Fig. 5). All factors taken together, conditions during the dry season result in heavier drip water $\delta^{13}C$ in Mawmluh Cave, whereas the opposite holds true for the ISM months.

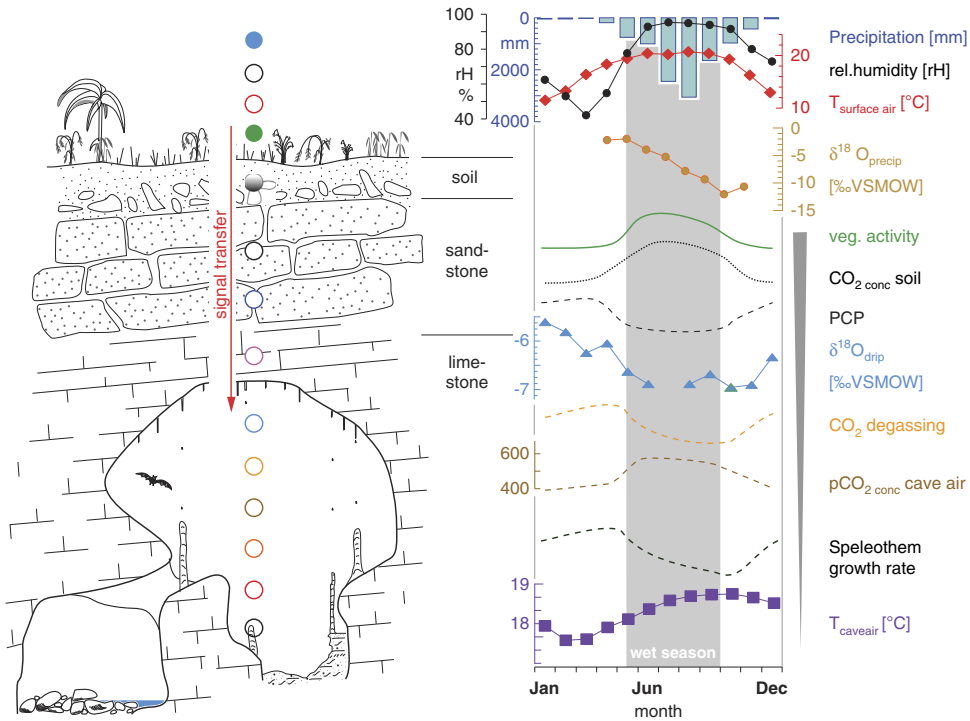

Figure 5. (color online) Schematic of the factors influencing isotope signals at Mawmluh Cave. Data are derived from monitoring studies at the cave site (Breitenbach et al., 2015), and precipitation data are from the Indian Meteorological Department Station Cherrapunji. VSMOW, Vienna standard mean ocean water. PCP, prior calcite precipitation.

https://doi.org/10.1017/qua.2017.72 Published online by Cambridge University Press

Drip water and stalagmite $\delta^{13}C$ are therefore strongly influenced by effective infiltration in the soil and tightly connected to local climate conditions.

Interpretation of the MAW-6 isotope records

We find large variations in $\delta^{18}O_{IVC}$ in stalagmite MAW-6 over the period of the last deglaciation, with the heaviest values recorded during the LG period and the YD (Fig. 3). Considering the controls on precipitation and drip water $\delta^{18}O_{IVC}$ at Mawmluh Cave, we interpret the LG and YD portions of the record as periods of weaker/shorter ISM, accompanied by changes in the circulation regime (i.e., a more proximal moisture source), whereas stronger ISM and longer moisture transport paths prevailed during the B-A and the Holocene. Changes in both SST and sea level because of the melting of the continental ice sheets during the last deglaciation resulted in substantial alteration of the isotopic composition of the surface ocean water and also affected evaporation and convection from the sea surface (Gadgil, 2003). The changes in the moisture source affect precipitation and stalagmite $\delta^{18}O$. In the BoB, the moisture source for the ISM, a ~3.2–3.5°C increase in SST between the last glacial maximum and the Holocene, and a +1.4°C SST shift between the YD and the Holocene have been documented (Rashid et al., 2007, 2011; Govil and Divakar Naidu, 2011). In this region, additional depletion of seawater ^{18}O occurred most likely because of freshening of the BoB by increased runoff from precipitation and glacier melt in the Himalaya and Tibet.

The millennial-scale average in MAW-6 $\delta^{13}C$ shows much lower variability than $\delta^{18}O_{IVC}$ over the last deglaciation, but the centennial-scale variations are remarkably similar (Fig. 3). It is likely that changes in vegetation density and composition occurred between cold/dry glacial and warm/humid interglacial periods. However, vegetation changes above the cave as the primary cause for the high frequency variation in $\delta^{13}C$ can probably be ruled out, as these would require longer time periods and would likely be more gradual than the rapid decadal-scale shifts we find in MAW-6. Karst processes—namely, PCP and kinetic fractionation in the cave—can best explain the observed variation in MAW-6 $\delta^{13}C$. We find heavier $\delta^{13}C$ values during weak ISM periods, as identified in the $\delta^{18}O_{IVC}$ record, indicating enhanced PCP and kinetic fractionation stemming from drier summer and/or longer winter seasons. Periods of strong ISM, on the other hand, are characterized by lighter $\delta^{13}C$ values, which is in line with more closed system conditions during the wet summers; higher cave air pCO_2, which subdues kinetic fractionation; and more active vegetation and soil.

It is possible that kinetic processes affect stalagmite $\delta^{18}O$ as well, precluding quantitative rainfall reconstructions, but still allowing qualitative interpretation of monsoon strength. In fact, kinetic fractionation would drive stalagmite $\delta^{18}O$ toward more positive values, as prolonged degassing and possibly evaporation enrich the precipitating solution in the heavy isotope, thus increasing the sensitivity of the speleothem to record dry periods. Modern drip water $\delta^{18}O$ values directly reflect precipitation $\delta^{18}O$ values at the site, lending additional confidence to the interpretation of stalagmite $\delta^{18}O$ as a monsoon strength proxy. Periods of enhanced kinetic fractionation in the past can be detected using the Hendy tests. Evidence for kinetic fractionation is observed during the YD and the LG, periods that we interpret as drier, whereas (near-)equilibrium conditions seem to have prevailed during the B-A and the Holocene, when conditions were wetter (Supplementary Fig. 1). These results have to be interpreted with care, however, as sampling along a single growth layer is extremely difficult when no annual laminae are present.

We can use the complementary information of $\delta^{18}O_{IVC}$ and $\delta^{13}C$ in stalagmite MAW-6 to interpret climate variations on supraregional and local scales over the last deglaciation. Clear shifts in average $\delta^{18}O_{IVC}$ are apparent during different time periods (clusters in Fig. 4), indicating changing ISM strength, related to the moisture source and composition upstream of the study site. Although shifts in $\delta^{13}C$ are less strongly expressed, it is still possible to distinguish periods of local aridity/humidity related to the amount of effective infiltration in the karst and cave ventilation dynamics. Positive correlation between $\delta^{18}O_{IVC}$ and $\delta^{13}C$ indicates that in general, weaker ISM conditions are reflected as locally drier conditions at the study site, because of either reduced summer rainfall or a prolonged dry season (Fig. 4). "Weak-ISM" periods (LG and YD) are also characterized by a tendency toward heavier $\delta^{13}C$, suggesting drier conditions at the cave site, whereas Holocene $\delta^{18}O_{IVC}$ and $\delta^{13}C$ clearly cluster at lighter values for both proxies, indicating strong ISM and humid conditions at the study site.

However, a detailed analysis of the relationship between $\delta^{18}O_{IVC}$ and $\delta^{13}C$ suggests that the connection between local climate and large-scale ISM dynamics might be more complex. The YD is clearly defined as the cluster with the heaviest $\delta^{18}O_{IVC}$ values, suggesting a more proximal moisture source with little freshwater influence from riverine runoff and an overall weakened ISM circulation (Fig. 4B). Local hydroclimate conditions (indicated by $\delta^{13}C$), on the other hand, appear to have been rather similar to those during the preceding B-A, but more arid than during the succeeding Holocene. This apparent inconsistency (weaker ISM, without increased aridity at local level) reflects the different controls on $\delta^{18}O_{IVC}$ and $\delta^{13}C$, where changes in the moisture source and composition do not necessarily always influence local infiltration directly (Cheng et al., 2016b). Although $\delta^{18}O_{IVC}$ is influenced primarily by the ISM during summer months, $\delta^{13}C$ is more sensitive to dry conditions (i.e., the arid winter months). However, the dry season months in Meghalaya are characterized by very dry conditions at present, and it is unlikely that conditions during the YD were much different (as drier than dry is impossible). It is thus likely that a change in precipitation seasonality during the YD led to a weaker ISM with a more proximal rainfall source during the summer months (i.e., heavier $\delta^{18}O_{IVC}$), and at the same time a more even distribution of rainfall over the year, resulting in

https://doi.org/10.1017/qua.2017.72 Published online by Cambridge University Press

reduced seasonality and little effective change in karst processes (i.e., lighter $\delta^{13}C$).

Comparison with other records from Mawmluh Cave

To test whether MAW-6 indeed reflects climate variations and not just local effects, we compared the MAW-6 $\delta^{18}O_{IVC}$ record with the KM-A record (Berkelhammer et al., 2012) and the MWS-1 record (Dutt et al., 2015) from the same cave (Fig. 6). We found good visual replication between the three records on a centennial time scale when recalculating the age models for KM-A and MWS-1 using COPRA (Fig. 6). The absolute difference in $\delta^{18}O$ values, especially pronounced between MAW-6 and MWS-1, was likely related to varying degrees of isotopic fractionation at different drip sites in the cave (similar to, e.g., Stoll et al., 2015). For more quantitative information, the three time series were interpolated to annual resolution and low-pass filtered in order to only consider centennial time scale variations. Correlations were then calculated by downsampling the data to 50-yr resolution. With this approach, we found high positive correlations between MAW-6 and KM-A during the period 6.9–9 ka ($r = 0.93$), as well as between 9 and 12.4 ka ($r = 0.78$, discarding the time periods corresponding to hiatuses in MAW-6). Similarly, correlation between MAW-6 and MWS-1 was positive ($r = 0.89$). All relationships were highly significant ($P < 10^{-9}$). Overall, this comparison corroborates our interpretation that variations in $\delta^{18}O_{IVC}$ in MAW-6 are driven by climate. The high resolution and the precise chronology of our record could significantly improve the available data from the ISM realm.

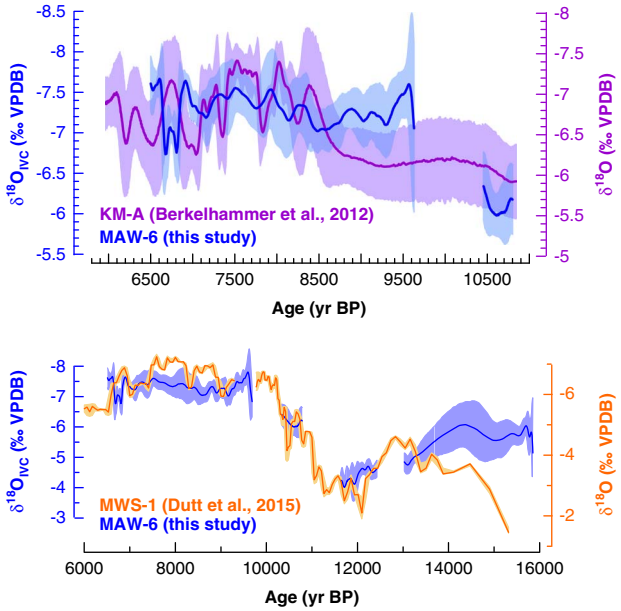

Figure 6. Comparison of stalagmite $\delta^{18}O$ records MAW-6 (blue), MWS-1 (orange; Dutt et al., 2015), and KM-A (purple; Berkelhammer et al., 2012). Proxy uncertainties (95% confidence intervals), as calculated by COPRA, are shown in light shading. $\delta^{18}O_{IVC}$, ice-volume-corrected $\delta^{18}O$; V-PDB, Vienna Pee Dee belemnite. (For interpretation of the references to color in this figure legend, the reader is referred to the web version of this article.)

Comparison with other AM records

We chose three high-resolution and precisely dated records from Chinese caves (Dongge: Dykoski et al., 2005; Yamen: Yang et al., 2010; Kulishu: Ma et al., 2012), the MWS-1 record from Mawmluh Cave, and the North Greenland Ice Core Project (NGRIP) ice core record from Greenland (Andersen et al., 2004) to compare with our MAW-6 $\delta^{18}O_{IVC}$ record (Fig. 7). Comparison of the MAW-6 $\delta^{18}O_{IVC}$ record with these reconstructions reveals very similar centennial-millennial scale trends over the last deglaciation, further corroborating our interpretation of the record as a proxy for ISM strength (Fig. 7). However, more subtle differences are apparent as well. For example, whereas the other AM reconstructions indicate the weakest summer monsoons during the last glacial period (until ~14.5 ka), reflecting the pattern found in Greenland ice cores, MAW-6 records the weakest ISM conditions during the YD (Fig. 7). This is partly related to the adopted correction for ice volume and SST, which results in lighter $\delta^{18}O_{IVC}$ during the last glacial period, but the pattern is also apparent in the original $\delta^{18}O$ record (Fig. 3). This is possibly a reflection of changes in regional seasonality in NE India, with a less vigorous ISM fed from proximal moisture sources, together with a wider spread of precipitation over the entire year during the YD. Testing this hypothesis requires seasonally resolved time series with highly robust chronologies.

In addition, differences appear when comparing the B-A interstadial period in MAW-6 with other records. Whereas the AM records considered here all show a relatively rapid transition at the beginning and the end of the interval, with a plateau of lighter $\delta^{18}O$ values during the B-A (attributed to increasing insolation; Ma et al., 2012), MAW-6 shows a pattern of rapid isotopic depletion at ~ 14.5 ka followed by a gradual increase toward YD values that is more similar to the transition recorded in Greenland ice cores (Fig. 7). This might hint toward a close connection between NE India and the North Atlantic realm, driven by the westerlies. Evidence from paleoclimate records from central Asia suggests that the AM and westerly climates are tightly connected over glacial-interglacial cycles (Cheng et al., 2016b). Mawmluh Cave is located close to the Tibetan Plateau, with frequent influence of dry air masses from the Tibetan High during the winter season, and a closer connection to the westerly climate than found at the Chinese cave sites is thus plausible. However, this interpretation needs to be cautiously evaluated because of limited replication with the other $\delta^{18}O$ record from Mawmluh Cave covering the B-A interval (MWS-1; Dutt et al., 2015), possibly related to chronological uncertainties in both records at this time.

The transition into the Holocene in MAW-6, although interrupted by a hiatus, shows substantially lighter $\delta^{18}O$ values and thus ISM strengthening over time, similar to the record from Yamen Cave (Yang et al., 2010) and

https://doi.org/10.1017/qua.2017.72 Published online by Cambridge University Press

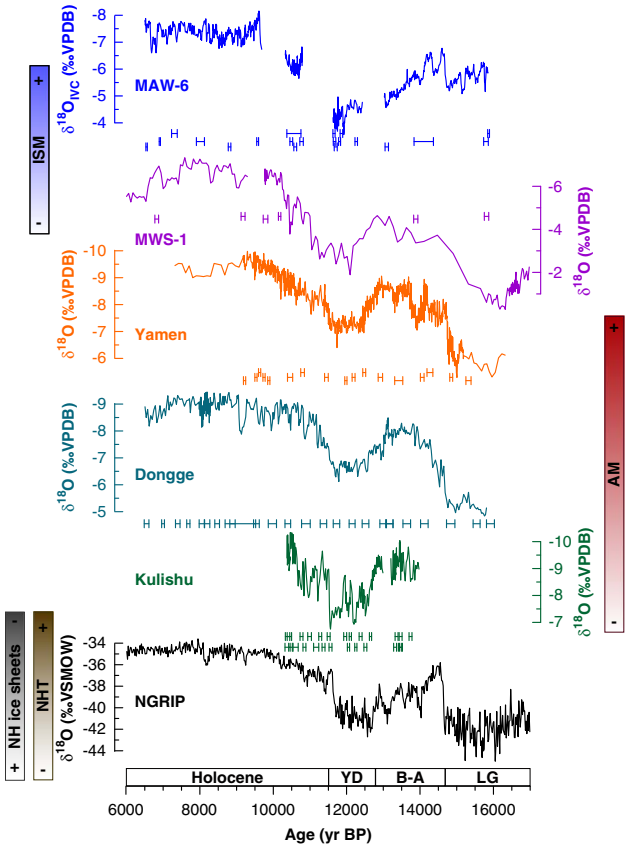

Figure 7. (color online) Comparison of MAW-6 ice-volume-corrected $\delta^{18}O$ ($\delta^{18}O_{IVC}$) with $\delta^{18}O$ records from the Indian summer monsoon (ISM) and broader Asian monsoon (AM) regions, as well as with the NGRIP ice core record. MAW-6 reflects and corroborates previous reconstructions from the AM region showing the weakest ISM after the deglaciation occurring during the Younger Dryas, and stronger ISM during the preceding Bølling-Allerød, as well as during the Holocene. VSMOW, Vienna standard mean ocean water; V-PDB, Vienna Pee Dee belemnite. NH, Northern Hemisphere; NHT, Northern Hemisphere Temperature.

well-replicated in MWS-1. Conversely to the gradually lighter $\delta^{18}O$ values found in the Yamen and Dongge cave records, however, both reconstructions from Mawmluh Cave show a short plateau of intermediate values between ~10.2 and 10.8 ka. In MAW-6, this interval is demarcated by two hiatuses; therefore, direct comparison with other records is difficult. This feature in the $\delta^{18}O$ records could reflect slow retreat or even a short-lived advance of the Himalayan glaciers, related to the increase in moisture and precipitation (strengthening ISM) at the onset of the Holocene (Meyer et al., 2009). The glaciation in the mountain range and related cold air outflow from the Himalaya mountain range would have hampered the intrusion of the ISM somewhat longer in NE India. This explanation remains hypothetical however, especially because of the scarcity of data from the region.

Dynamic changes in the ISM

Dynamic regime changes in the ISM between the LG period and the EH were investigated using recurrence quantification analysis (Ozken et al., 2015; Eroglu et al., 2016). We found a significant regime transition between LG and EH ISM, with more chaotic conditions during the LG, but higher predictability during the EH (Fig. 8). Disruption and weakening of the ISM during the LG, with frequent influence from westerly air masses and the Tibetan High, very likely result in less predictable conditions. This is similar to findings from complex network analysis of the AM, where weaker suprarregional links were found during the cold/dry Little Ice Age (100–400 yr BP), suggesting that a weaker ISM is less predictable on a regional scale (Rehfeld et al., 2012). During the EH, on the other hand, the strong seasonality induced by the ISM would lead to more regular annual cycles in precipitation and to a higher predictability.

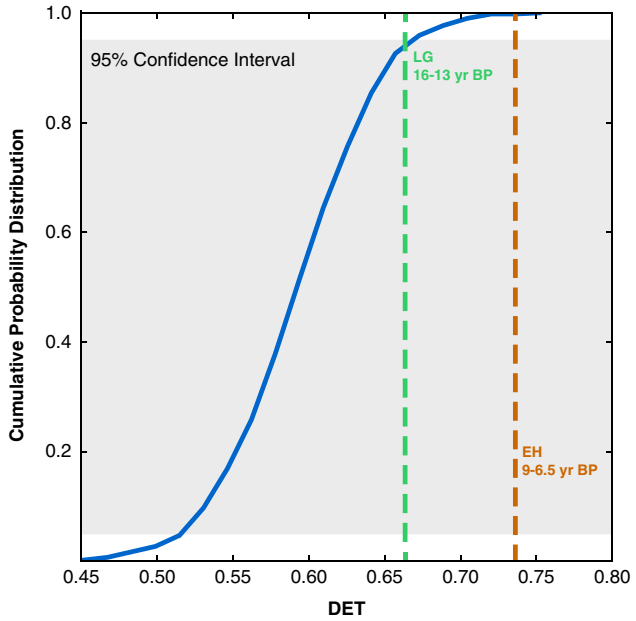

Figure 8. Results of the TACTS analysis on MAW-6 $\delta^{18}O$. The cumulative probability distribution established through 5000 random realizations of recurrence determinism (DET) measure is shown by the blue line, with gray shading indicating the 95% confidence interval. The late glacial (LG) period and early Holocene (EH) are characterized by distinct DET measures (0.663 and 0.736, respectively). Although the LG is within the 95% confidence interval, the EH is outside, highlighting the high predictability of the Indian summer monsoon during this period. (For interpretation of the references to color in this figure legend, the reader is referred to the web version of this article.)

CONCLUSIONS

Stalagmite MAW-6 provides new paleoclimate data from Mawmluh Cave in NE India, covering the last deglaciation. We combine decadal-scale $\delta^{18}O$ and $\delta^{13}C$ measurements on MAW-6 to unravel climate change at regional and local scales over this period. A substantial postglacial shift toward more negative $\delta^{18}O$ values is interpreted as strengthening of the ISM, with maximum expression during the EH. This pattern is in agreement with other reconstructions from

https://doi.org/10.1017/qua.2017.72 Published online by Cambridge University Press

Mawmluh Cave and the AM realm. Both the B-A and YD periods are clearly demarcated in the record as stronger and weaker ISM, respectively. $\delta^{13}C$ is interpreted as reflecting local hydroclimatic conditions and is generally similar to $\delta^{18}O$, suggesting that a weak/strong ISM results in drier/wetter conditions at the study site. An intriguing exception to this rule is the YD, where combined $\delta^{18}O$ and $\delta^{13}C$ analysis suggests a reduction in precipitation seasonality, together with weakening of the ISM. Statistical time series analysis of the $\delta^{18}O$ record reveals a significant regime transition over the last deglaciation, with less predictable ISM during the LG period and higher predictability during the Holocene, which we relate to the buildup of strong precipitation seasonality induced by the ISM.

ACKNOWLEDGMENTS

We gratefully acknowledge financial support from the Swiss National Fond (SNF Sinergia grant CRSI22 132646/1 and grant P2EZP2_172213), the German Science Foundation (DFG project MA4759/8-1—Impacts of uncertainties in climate data analysis [IUCliD]: approaches to working with measurements as a series of probability distributions—and grant no. RE3994-1/1), the National Natural Science Foundation of China (NSFC) grants 4123054 and 2013CB955902, the U.S. National Science Foundation grant 1103403, and the European Union's Horizon 2020 Research and Innovation program under the Marie Skłodowska-Curie grant agreement no. 691037 (QUEST). We thank our Indian colleagues Bijay Mipun and Gregory Diengdoh for their logistic help. We thank Daniel Gebauer for support during fieldwork. We also thank Lydia Zehnder and Stewart Bishop (both at ETH Zürich) for assistance during XRD and stable isotope analysis, respectively. Tim Eglinton is acknowledged for financial support of F.A.L. We thank Ashish Sinha, Max Berkelhammer, James Baldini, Yanjun Cai, and two anonymous reviewers for constructive feedback and fruitful discussions on this and earlier versions of this manuscript. We thank the editors, Matthew Lachniet and Lewis Owen, for feedback and handling of the manuscript.

SUPPLEMENTARY MATERIAL

For supplementary material/s referred to in this article, please visit https://doi.org/10.1017/qua.2017.72

REFERENCES

Andersen, K.K., Azuma, N., Barnola, J.-M., Bigler, M., Biscaye, P., Caillon, N., Chappellaz, J., et al., 2004. High-resolution record of Northern Hemisphere climate extending into the last interglacial period. *Nature* 431, 147–151.

Baker, A.J., Sodemann, H., Baldini, J.U.L., Breitenbach, S.F.M., Johnson, K.R., van Hunen, J., Pingzhong, Z., 2015. Seasonality of westerly moisture transport in the East Asian summer monsoon and its implications for interpreting precipitation $\delta^{18}O$. *Journal of Geophysical Research: Atmospheres* 120, 5850–5862.

Baldini, J.U.L., 2010. Cave atmosphere controls on stalagmite growth rate and palaeoclimate records. *Geological Society, London, Special Publications* 336, 283–294.

Baldini, L.M., Baldini, J.U.L., McElwaine, J.N., Frappier, A.B., Asmerom, Y., Liu, K., Prufer, K.M., et al., 2016. Persistent northward North Atlantic tropical cyclone track migration over the past five centuries. *Scientific Reports* 6, 37522. http://dx.doi.org/10.1038/srep37522.

Berkelhammer, M., Sinha, A., Stott, L., Cheng, H., Pausata, F.S.R., Yoshimura, K., 2012. An abrupt shift in the Indian monsoon 4000 years ago. *Geophysical Monograph Series* 198, 75–87.

Breitenbach, S.F.M., Adkins, J.F., Meyer, H., Marwan, N., Kumar, K.K., Haug, G.H., 2010. Strong influence of water vapor source dynamics on stable isotopes in precipitation observed in southern Meghalaya, NE India. *Earth and Planetary Science Letters* 292, 212–220.

Breitenbach, S.F.M., Bernasconi, S.M., 2011. Carbon and oxygen isotope analysis of small carbonate samples (20 to 100 µg) with a GasBench II preparation device. *Rapid Communications in Mass Spectrometry* 25, 1910–1914.

Breitenbach, S.F.M., Lechleitner, F.A., Meyer, H., Diengdoh, G., Mattey, D., Marwan, N., 2015. Cave ventilation and rainfall signals in dripwater in a monsoonal setting – a monitoring study from NE India. *Chemical Geology* 402, 111–124.

Breitenbach, S.F.M., Rehfeld, K., Goswami, B., Baldini, J.U.L., Ridley, H.E., Kennett, D.J., Prufer, K.M., et al., 2012. Constructing proxy records from age models (COPRA). *Climate of the Past* 8, 1765–1779.

Burns, S.J., Fleitmann, D., Mudelsee, M., Neff, U., Matter, A., Mangini, A., 2002. A 780-year annually resolved record of Indian Ocean monsoon precipitation from a speleothem from south Oman. *Journal of Geophysical Research: Atmospheres* 107, 4434. http://dx.doi.org/10.1029/2001JD001281.

Cheng, H., Edwards, R.L., Broecker, W.S., Denton, G.H., Kong, X., Wang, Y., Zhang, R., Wang, X., 2009. Ice age terminations. *Science* 326, 248–252.

Cheng, H., Edwards, R.L., Hoff, J., Gallup, C.D., Richards, D.A., Asmerom, Y., 2000. The half-lives of uranium-234 and thorium-230. *Chemical Geology* 169, 17–33.

Cheng, H., Edwards, R.L., Shen, C.C., Polyak, V.J., Asmerom, Y., Woodhead, J., Hellstrom, J., et al., 2013. Improvements in ^{230}Th dating, ^{230}Th and ^{234}U half-life values, and U–Th isotopic measurements by multi-collector inductively coupled plasma mass spectrometry. *Earth and Planetary Science Letters* 371–372, 82–91.

Cheng, H., Edwards, R.L., Sinha, A., Spötl, C., Yi, L., Chen, S., Kelly, M., et al., 2016a. The Asian monsoon over the past 640,000 years and ice age terminations. *Nature* 534, 640–646.

Cheng, H., Spötl, C., Breitenbach, S.F.M., Sinha, A., Wassenburg, J.A., Jochum, K.P., Scholz, D., et al., 2016b. Climate variations of Central Asia on orbital to millennial timescales. *Scientific Reports* 6, 36975. http://dx.doi.org/10.1038/srep36975.

Cosford, J., Qing, H., Mattey, D., Eglington, B., Zhang, M., 2009. Climatic and local effects on stalagmite $\delta^{13}C$ values at Lianhua Cave, China. *Palaeogeography, Palaeoclimatology, Palaeoecology* 280, 235–244.

Dansgaard, W., 1964. Stable isotopes in precipitation. *Tellus* 16, 436–468.

Denniston, R.F.Y., Gonzalez, L.A., Asmerom, Y., Polyak, V., 2001. A high-resolution speleothem record of climatic variability at the Allerød–Younger Dryas transition in Missouri, central United States. *Palaeogeography, Palaeoclimatology, Palaeoecology* 176, 147–155.

Dutt, S., Gupta, A.K., Clemens, S.C., Cheng, H., Singh, R.K., Kathayat, G., Edwards, R.L., 2015. Abrupt changes in Indian

summer monsoon strength during 33,800 to 5500 years B.P. *Geophysical Research Letters* 42, 5526–5532.

Dykoski, C.A., Edwards, R.L., Cheng, H., Yuan, D., Cai, Y., Zhang, M., Lin, Y., Qing, J., An, Z., Revenaugh, J., 2005. A high-resolution, absolute-dated Holocene and deglacial Asian monsoon record from Dongge Cave, China. *Earth and Planetary Science Letters* 233, 71–86.

Edwards, R.L., Chen, J.H., Wasserburg, G.J., 1987. ^{238}U–^{234}U–^{230}Th–^{232}Th systematics and the precise measurement of time over the past 500,000 years. *Earth and Planetary Science Letters* 81, 175–192.

Eroglu, D., McRobie, F.H., Ozken, I., Stemler, T., Wyrwoll, K.-H., Breitenbach, S.F.M., Marwan, N., Kurths, J., 2016. See-saw relationship of the Holocene East Asian–Australian summer monsoon. *Nature Communications* 7, 12929. http://dx.doi.org/10.1038/ncomms12929.

Fairchild, I.J., Baker, A., 2012. *Speleothem Science: From Process to Past Environments*. Wiley-Blackwell, Chichester, West Sussex, UK.

Fleitmann, D., Burns, S.J., Mangini, A., Mudelsee, M., Kramers, J., Villa, I., Neff, U., et al., 2007. Holocene ITCZ and Indian monsoon dynamics recorded in stalagmites from Oman and Yemen (Socotra). *Quaternary Science Reviews* 26, 170–188.

Gadgil, S., 2003. The Indian monsoon and its variability. *Annual Review of Earth and Planetary Sciences* 31, 429–467.

Gebauer, H.D., 2008. Resources on the speleology of Meghalaya state, India. Part 1: overview. *Berliner Höhlenkundliche Berichte* 33, 152.

Genty, D., Baker, A., Massault, M., Proctor, C., Gilmour, M., Pons-Branchu, E., Hamelin, B., 2001. Dead carbon in stalagmites: carbonate bedrock paleodissolution vs. ageing of soil organic matter. *Implications for ^{13}C variations in speleotherms. Geochimica et Cosmochimica Acta* 65, 3443–3457.

Genty, D., Blamart, D., Ghaleb, B., Plagnes, V., Causse, C., Bakalowicz, M., Zouari, K., et al., 2006. Timing and dynamics of the last deglaciation from European and North African $\delta^{13}C$ stalagmite profiles—comparison with Chinese and South Hemisphere stalagmites. *Quaternary Science Reviews* 25, 2118–2142.

Genty, D., Blamart, D., Ouahdi, R., Gilmour, M., Baker, A., Jouzel, J., Van-Exter, S., 2003. Precise dating of Dansgaard-Oeschger climate oscillations in western Europe from stalagmite data. *Nature* 421, 833–837.

Ghosh, S., Fallick, A.E., Paul, D.K., Potts, P.J., 2005. Geochemistry and origin of neoproterozoic granitoids of Meghalaya, northeast India: implications for linkage with amalgamation of Gondwana supercontinent. *Gondwana Research* 8, 421–432.

Govil, P., Divakar Naidu, P., 2011. Variations of Indian monsoon precipitation during the last 32 kyr reflected in the surface hydrography of the western Bay of Bengal. *Quaternary Science Reviews* 30, 3871–3879.

Griffiths, M.L., Fohlmeister, J., Drysdale, R.N., Hua, Q., Johnson, K.R., Hellstrom, J.C., Gagan, M.K., Zhao, J.X., 2012. Hydrological control of the dead carbon fraction in a Holocene tropical speleothem. *Quaternary Geochronology* 14, 81–93.

Hendy, C.H., 1971. The isotopic geochemistry of speleothems—I. The calculation of the effects of different modes of formation on the isotopic composition of speleothems and their applicability as palaeoclimatic indicators. *Geochimica et Cosmochimica Acta* 35, 801–824.

Kathayat, G., Cheng, H., Sinha, A., Spötl, C., Edwards, R.L., Zhang, H., Li, X., et al., 2016. Indian monsoon variability on millennial-orbital timescales. *Scientific Reports* 6, 24374. http://dx.doi.org/10.1038/srep24374.

Lawrence, J.R., Gedzelman, S.D., Dexheimer, D., Cho, H.-K., Carrie, G.D., Gasparini, R., Anderson, C.R., Bowman, K.P., Biggerstaff, M.I., 2004. Stable isotopic composition of water vapor in the tropics. *Journal of Geophysical Research: Atmospheres* 109, D06115. http://dx.doi.org/10.1029/2003JD004046.

Ma, Z.B., Cheng, H., Tan, M., Edwards, R.L., Li, H.C., You, C.F., Duan, W.H., Wang, X., Kelly, M.J., 2012. Timing and structure of the Younger Dryas event in northern China. *Quaternary Science Reviews* 41, 83–93.

Marwan, N., Romano, M.C., Thiel, M., Kurths, J., 2007. Recurrence plots for the analysis of complex systems. *Physics Reports* 438, 237–329.

Menzel, P., Gaye, B., Mishra, P.K., Anoop, A., Basavaiah, N., Marwan, N., Plessen, B., et al., 2014. Linking Holocene drying trends from Lonar Lake in monsoonal central India to North Atlantic cooling events. *Palaeogeography, Palaeoclimatology, Palaeoecology* 410, 164–178.

Meyer, M.C., Hofmann, C.-C., Gemmell, A.M.D., Haslinger, E., Häusler, H., Wangda, D., 2009. Holocene glacier fluctuations and migration of Neolithic yak pastoralists into the high valleys of northwest Bhutan. *Quaternary Science Reviews* 28, 1217–1237.

Murata, F., Terao, T., Hayashi, T., Asada, H., Matsumoto, J., 2008. Relationship between atmospheric conditions at Dhaka, Bangladesh, and rainfall at Cherrapunjee, India. *Natural Hazards* 44, 399–410.

Myers, C.G., Oster, J.L., Sharp, W.D., Bennartz, R., Kelley, N.P., Covey, A.K., Breitenbach, S.F.M., 2015. Northeast Indian stalagmite records Pacific decadal climate change: implications for moisture transport and drought in India. *Geophysical Research Letters* 42, 4124–4132.

Oster, J.L., Montañez, I.P., Kelley, N.P., 2012. Response of a modern cave system to large seasonal precipitation variability. *Geochimica et Cosmochimica Acta* 91, 92–108.

Ozken, I., Eroglu, D., Stemler, T., Marwan, N., Bagci, G.B., Kurths, J., 2015. Transformation-cost time-series method for analyzing irregularly sampled data. *Physical Review E* 91, 062911. http://dx.doi.org/10.1103/PhysRevE.91.062911.

Pausata, F.S.R., Battisti, D.S., Nisancioglu, K.H., Bitz, C.M., 2011. Chinese stalagmite $\delta^{18}O$ controlled by changes in the Indian monsoon during a simulated Heinrich event. *Nature Geoscience* 4, 474–480.

Prokop, P., Walanus, A., 2003. Trends and periodicity in the longest instrumental rainfall series for the area of most extreme rainfall in the world, northeast India. *Geographia Polonica* 76, 25–35.

Rashid, H., England, E., Thompson, L., Polyak, L., 2011. Late glacial to Holocene Indian summer monsoon variability based upon sediment. *Terrestrial, Atmospheric, and Oceanic Sciences* 22, 215–228.

Rashid, H., Flower, B.P., Poore, R.Z., Quinn, T.M., 2007. A ~25 ka Indian Ocean monsoon variability record from the Andaman Sea. *Quaternary Science Reviews* 26, 2586–2597.

Rehfeld, K., Kurths, J., 2014. Similarity estimators for irregular and age-uncertain time series. *Climate of the Past* 10, 107–122.

Rehfeld, K., Marwan, N., Breitenbach, S.F.M., Kurths, J., 2012. Late Holocene Asian summer monsoon dynamics from small but complex networks of palaeoclimate data. *Climate Dynamics* 41, 3–19.

Ridley, H.E., Asmerom, Y., Baldini, J.U.L., Breitenbach, S.F.M., Aquino, V.V., Prufer, K.M., Culleton, B.J., et al., 2015. Aerosol forcing of the position of the intertropical convergence zone since AD 1550. *Nature Geoscience* 8, 195–200.

Scholz, D., Frisia, S., Borsato, A., Spötl, C., Fohlmeister, J., Mudelsee, M., Miorandi, R., Mangini, A., 2012. Holocene climate variability in north-eastern Italy: potential influence of the NAO and solar activity recorded by speleothem data. *Climate of the Past* 8, 1367–1383.

Sengupta, S., Sarkar, A., 2006. Stable isotope evidence of dual (Arabian Sea and Bay of Bengal) vapour sources in monsoonal precipitation over north India. *Earth and Planetary Science Letters* 250, 511–521.

Shakun, J.D., Clark, P.U., He, F., Marcott, S.A., Mix, A.C., Liu, Z., Otto-Bliesner, B., Schmittner, A., Bard, E., 2012. Global warming preceded by increasing carbon dioxide concentrations during the last deglaciation. *Nature* 484, 49–54.

Singh, M., Singh, I.B., Müller, G., 2007. Sediment characteristics and transportation dynamics of the Ganga River. *Geomorphology* 86, 144–175.

Sinha, A., Cannariato, K.G., Stott, L.D., Cheng, H., Edwards, R.L., Yadava, M.G., Ramesh, R., Singh, I.B., 2007. A 900-year (600 to 1500 A.D.) record of the Indian summer monsoon precipitation from the core monsoon zone of India. *Geophysical Research Letters* 34, L16707. http://dx.doi.org/10.1029/2007GL030431.

Sinha, A., Cannariato, K.G., Stott, L.D., Li, H.C., You, C.F., Cheng, H., Edwards, R.L., Singh, I.B., 2005. Variability of southwest Indian summer monsoon precipitation during the Bølling-Ållerød. *Geology* 33, 813–816.

Stoll, H., Mendez-Vicente, A., Gonzalez-Lemos, S., Moreno, A., Cacho, I., Cheng, H., Edwards, R.L., 2015. Interpretation of orbital scale variability in mid-latitude speleothem $\delta^{18}O$: significance of growth rate controlled kinetic fractionation effects. *Quaternary Science Reviews* 127, 215–228.

Wang, Y., Cheng, H., Edwards, R.L., He, Y., Kong, X., An, Z., Wu, J., Kelly, M.J., Dykoski, C.A., Li, X., 2005. The Holocene Asian monsoon: links to solar changes and North Atlantic climate. *Science* 308, 854–857.

Wang, Y.J., Cheng, H., Edwards, R.L., An, Z.S., Wu, J.Y., Shen, C.C., Dorale, J.A., 2001. A high-resolution absolute-dated late Pleistocene monsoon record from Hulu Cave, China. *Science* 294, 2345–2348.

Webster, P.J., 2013. Improve weather forecasts for the developing world. *Nature* 493, 17–19.

Yang, Y., Yuan, D.X., Cheng, H., Zhang, M.L., Qin, J.M., Lin, Y.S., Zhu, X.Y., Edwards, R.L., 2010. Precise dating of abrupt shifts in the Asian Monsoon during the last deglaciation based on stalagmite data from Yamen Cave, Guizhou Province, China. Science China Earth Sciences. 53, 633–641.

Yuan, D., Cheng, H., Edwards, R.L., Dykoski, C.A., Kelly, M.J., Zhang, M., Qing, J., et al., 2004. Timing, duration, and transitions of the last interglacial Asian monsoon. *Science* 304, 575–578.

Zhisheng, A., Clemens, S.C., Shen, J., Qiang, X., Jin, Z., Sun, Y., Prell, W.L., et al., 2011. Glacial-interglacial Indian summer monsoon dynamics. *Science* 333, 719–723.

https://doi.org/10.1017/qua.2017.72 Published online by Cambridge University Press